Closed-form solution for the length of drip laterals and easy selection of commercial emitters for low-slope fields under the Hazen-Williams and Blasius resistance equations

Journal:	*Irrigation and Drainage*
Manuscript ID	IRD-23-0320.R2
Wiley - Manuscript type:	Research Article
Date Submitted by the Author:	n/a
Complete List of Authors:	Baiamonte, Giorgio; University of Palermo, Department of Agricultural, Food And Forest Sciences (SAAF)
Keywords:	drip irrigation, analytical solution, commercial emitters, minor losses

Closed-form solution for the length of drip laterals and easy selection of commercial emitters for low-slope fields under the Hazen-Williams and Blasius resistance equations

Giorgio Baiamonte

Department of Agricultural, Food and Forest Sciences (SAAF), University of Palermo, Viale delle Scienze, Bldg 4, 90128 Palermo, Italy.

Correspondence

Giorgio Baiamonte, Department of Agricultural, Food and Forest Sciences (SAAF), University of Palermo, Viale delle Scienze, Bldg 4, 90128 Palermo, Italy. Email: giorgio.baiamonte@unipa.it

Abstract

This paper proposes a simple method for determining drip lateral length in relatively flat fields in which minor losses are not considered and a uniform emitter flow rate is assumed. This makes it possible to derive a useful relationship in a closed-form to determine drip lateral length according to the Hazen-Williams and Blasius resistance equations. An important advantage of the proposed procedure for determining drip lateral length is that it helps users establish the characteristics of the commercial emitters that they should select, an issue that has been poorly addressed in the past. Finally, after deriving this new solution, the same relationship is extended to a case in which minor losses are considered, and the uniform emitters' flow rate assumption is relaxed. The results of all input datasets show that when neglecting minor losses, the relative error between the inlet pressure head estimated with the suggested procedure and that calculated with the exact numerical method is less than 2.5%. However, when minor losses are considered, the number of emitters must not exceed 300 to obtain this threshold error. Several applications are performed, showing the reliability of this new design procedure.

Keywords: microirrigation, analytical solution, commercial emitters, minor losses

Résumé

Cet article propose une méthode simple pour déterminer la longueur latérale d'égouttement dans des champs relativement plats, dans laquelle les pertes mineures ne sont pas prises en compte et un débit d'émetteur uniforme est supposé. Cela permet de dériver une relation utile sous forme fermée pour déterminer la longueur du latérale, selon les équations de résistance de Hazen-Williams et Blasius. Un avantage important de la procédure proposée pour déterminer la longueur latérale est qu'elle aide les utilisateurs à établir les caractéristiques des émetteurs commerciaux qu'ils devraient sélectionner, une question qui a été mal abordée dans le passé. Finalement, après avoir dérivé cette nouvelle solution, la même relation est étendue à un cas dans lequel des pertes mineures sont considérées, et l'hypothèse de débit uniforme des émetteurs est assouplie. Les résultats de tous les ensembles de données d'entrée montrent qu'en négligeant les pertes mineures, l'erreur relative entre la hauteur de pression d'entrée estimée avec la procédure suggérée et celle calculée avec la méthode numérique exacte est inférieure à 2.5%. Cependant, lorsque l'on considère des pertes mineures, le nombre d'émetteurs ne doit pas dépasser 300 pour obtenir ce seuil d'erreur. Plusieurs applications sont réalisées, démontrant la fiabilité de cette nouvelle procédure de conception.

MOTS CLÉS: irrigation goutte à goutte, solution analytique, émetteurs commerciaux, pertes mineures

Introduction

Many studies have shown that drip irrigation significantly increases crop yield and enhances water use efficiency compared with conventional irrigation systems (Liu et al., 2013; Shareef et al., 2019). Despite its well-known advantages, drip irrigation accounts for only approximately 4% of the total global irrigation (Foley et al., 2011; Friedlander et al., 2013) and is expected to increase due to water scarcity and its ability to reduce water losses (Singh, 2022; Rodell and Li, 2023).

During recent decades, the scientific community has put much effort into improving methods to design trickle irrigation systems to encourage the choice of this water-saving irrigation system (Valiantzas, 1998, Baiamonte, 2018a, 2018b).

A widely debated topic in academic discourse is the advantages of using simplified analytical design methods instead of exact numerical procedures. Regardless of where one stands in this debate, the usefulness of closed-form solutions is evident since they can help provide important insights before implementing more time-consuming numerical methods (Kang and Nishiyama, 1996). In drip irrigation, as in many other contexts regarding fluid dynamics (such as the runoff generation process or the water transportation process in porous media), the availability of closed-form should be emphasized. This is because simple closed-form relationships show that parameter interactions result in the desired emission uniformity (Karmeli and Keller, 1975), thus allowing users to identify the most convenient design choices while also considering the actual availability of commercial materials.

Warrick and Yitayew (1988) derived analytical solutions that include a spatially variable discharge function in their basic derivation, accounting for the possibility of a variable emitter flow rate. In a companion paper, Yitayew and Warrick (1988) compared the results of their model to experimental measurements and provided an example that includes a manufacturer's variability component.

More recently, by using an explicit formula for the Darcy–Weisbach equation, Dercas and Valiantzas (2012) presented two explicit design methods for simple irrigation delivery systems. In the first method, the authors provided a simple equation to calculate the discharge corresponding to the available pipe diameters. In the second method, the optimum economic diameter could be calculated for every pipeline of the network.

For one-lateral units, Baiamonte (2018a) derived design relationships for horizontal and sloped laterals by neglecting emitter flow rate variations and minor losses. However, these relationships are based on calibrated numerical constants that, despite providing negligible errors in estimating the design variables, are affected by the sampling point location on which a closed-form solution would not depend on; this is why the latter should be preferred. Later, these calibrated relationships were extended to drip irrigation subunits (Baiamonte, 2018b), which can be applied to any laterals and manifold slopes. The software IrriLab was also developed to facilitate the design.

To further advance the progress in drip irrigation design described above, this paper proceeds with three main objectives. The first objective of this paper is to improve the procedure for horizontal lateral design developed by Baiamonte (2018a) by providing closed-form solutions with no calibration. The second objective of this study was to adapt this procedure to design drip laterals according to commercial emitter characteristics. Finally, the third and final objective of this work is to investigate the effect of minor losses and uniform emitter flow rate assumptions on the design variables established by the proposed method. After describing the sketch of the drip lateral where the design parameters are defined, the paper is organized into separate sections where the assumptions of neglecting or not neglecting the emitter flow rate uniformity and the minor losses are considered. Applications and discussions are included in each section.

Sketch of the drip lateral

Consider a drip lateral where j (j = 1, 2, …, N) non-pressure compensating emitters (N-PCE) with a spacing of S (m) are installed. The lateral length is $L = S\,N$, with emitters numbered from the downstream (**Fig. 1**), where the abscissa is $X = 0$ and the pressure head is the minimum, h_{min} (m). At the inlet ($X = L$), the discharge is q_{in} (L/h), and the pressure head equals h_{in} (m), which matches the maximum pressure head h_{max} (m).

Figure 1: ABOUT HERE.

By assuming a uniform emitter flow rate, q_n (L h^{-1}), the inlet flow rate, q_{in}, would be $N\, q_n$ (**Fig. 1**). For N-PCE emitters, which are characterized by k_e (L h^{-1} m^{-x}) and x parameters, the emitter flow rate is governed by the well-known emitter flow relation $q = k_e\, h^x$ (Singh and Su 2022). Nevertheless, this work will show that neglecting the emitter flow relation provides acceptable errors when considering N-PCE emitters if: i) the pressure head tolerance, δ (dimensionless), is sufficiently small (**Fig. 1**) and ii) the uniform flow rate to be selected for the emitters, q_n, is associated with the nominal (average) pressure head, $h_n = 0.5\,(h_{in} + h_{min})$, derived by the emitter flow relation ($q_n = k_e\, h_n^x$). Of course, the latter can also be written in the inverted form that will be used later:

$$h_n = \left(\frac{q_n}{k_e}\right)^{1/x} \quad (1)$$

Note that q_n in Eq. (1) is a constant in agreement with the uniform flow rate assumption. The two abovementioned conditions can be observed in **Fig. 2**, where for k_e = 0.69 L h^{-1} m^{-x} and x = 0.5, the emitter flow relation (Eq. 1) is plotted.

Figure 2: ABOUT HERE.

For a small pressure head tolerance such as the usually assumed δ = 10% (Wu, 1992; Wu et al., 1979; Baiamonte, 2016a, 2016b), **Fig. 2** demonstrates the linearity and narrow range of emitter flow rates associated with the emitter flow relation. The narrow range [h_{min}, h_{in}] is delimited by h_{min} and by h_{in} to be applied at the inlet (**Fig. 1**):

$$h_{min} = (1-\delta)\, h_n \le h_j \le (1+\delta)\, h_n = h_{in} \quad (2)$$

where h_n (which equals 20 m in **Fig. 2**) is the nominal (average) emitter pressure head that, for fixed δ, can be expressed by h_{min} or by h_{in}:

$$h_n = \frac{h_{min}}{(1-\delta)} = \frac{h_{in}}{(1+\delta)} \quad (3)$$

In **Fig. 2**, the extreme pressure head values [h_{min}, h_{in}] established by δ are indicated, delimiting the admissible range of variability of the emitters' pressure heads under the assumption of a uniform emitter flow rate (PCE). In Eq. (3), the corresponding pressure head tolerance is expressed as a function of h_{in} and h_{min}:

$$\delta = \frac{h_{in} - h_{min}}{h_{in} + h_{min}} \quad (4)$$

Note that imposing pressure head tolerance, δ, also entails imposing the Karmeli and Keller's (1975) emission uniformity, EU, since it was shown that δ and EU are linked by a simple linear relationship (Baiamonte, 2018a; Baiamonte et al., 2024).

When applying this procedure based on the assumption of uniform emitter flow rates (q_n = 3.1 L/h = const, in **Fig. 2**) to N-PCEs, an error is expected in the calculation of the inlet pressure head, h_{in}, compared to a calculation by the step-by-step (SBS) method. Indeed, SBS accounts for the emitter flow relation and is based on the repetitive application of the basic hydraulic equations (motion and continuity) that are applied to consecutive emitters. Thus, SBS represents the most exact method for estimating the pressure heads and the actual flow rates of the emitters on the laterals. It is expected that the margin of error between the results from the proposed procedure and the SBS procedure increases with increasing δ and for very low pressure heads when the linearity of the emitter flow relation vanishes (**Fig. 2**).

The next section shows that i) assuming uniform emitter flow rates makes it possible to determine a new formula that is easy to apply and ii) it results in small errors when it is used for N-PCEs, provided that the pressure head tolerance is small. The effect of local losses is addressed in the subsequent section.

Neglecting local losses (uniform emitter flow rate)

When neglecting local losses, under a uniform emitter flow rate (x = 0), the energy balance equation applied to the drip lateral can be written as (Baiamonte, 2018a):

$$h_j = h_{min} + K\,S\,H(j-1,-r) \quad (5)$$

where the K parameter accounts for friction losses (friction head loss gradient) along the laterals, S (m) is the emitters' interspacing, and $H(j-1, -r)$ is the generalized harmonic number of order $-r$, truncated at $j-1$ (Abramowitz and Stegun, 1965):

$$H(j-1,-r) = \sum_{i=1}^{j}(i-1)^r \quad (6)$$

Of course, for $j = 1$, $H(0, -r) = 0$, and by Eq. (5), $h_1 = h_{min}$. The friction head loss gradient, K, can be expressed according to the following monomial power law:

$$K = k\frac{q_n^r}{D^s} \quad (7)$$

where k, r and s need to be differently determined using the Blasius' or Hazen-Williams' resistance equations, which are both widely accepted for the smooth-walled polyethylene pipe (Keller and Bliesner, 1990) usually used in drip irrigation:

$$k = k_{BL} = \frac{0.316\ 2^{2.5}}{g\ \pi^{1.75}} \nu^{0.25} \qquad r = 1.75, s = 4.75 \quad Blasius\ eq. \tag{8}$$

$$k = k_{HW} = \frac{10.675}{C^r} \qquad r = 1.852, s = 4.871 \quad Hazen-Williams\ eq. \tag{9}$$

where ν is the water kinematic viscosity equal to 1.008 10^{-6} m^2 s^{-1} for a standard water temperature of 20 °C and C is the pipe smoothness factor, which in this work will be assumed to be equal to 135 (Moghazi, 1998) for polyethylene pipes. Note that although the Blasius and Hazen–Williams resistance equations are used here, the procedure can also be applied with any other resistance formula.

To obtain h_{in}, $j = N + 1$ needs to be set (**Fig. 1**) into Eq. (5), providing:

$$h_{in} = h_{min} + K\ S\ H(N, -r) \tag{10}$$

Eq. (5) and Eq. (10) are easy to apply when preassigning the desired length of the lateral, and one wants to determine the pressure head distribution (PHD) until the maximum pressure head, h_{in}, is reached. However, for an assigned inlet pressure head, h_{in}, and emitter interspace, S, the number of emitters or the length of the lateral ($L = S\ N$) may be unknown and thus cannot be derived by Eq. (10). This issue, which may also be of interest to manufacturers when publishing catalogues, can be solved as follows.

Substituting Eq. (6) into Eq. (5) gives:

$$h_j = h_{min} + k\frac{q_n^r}{D^s} S \sum_{j=1}^{j} (j-1)^r \tag{11}$$

We can switch from discrete to continuous integration by introducing the continuous variable $j_* = 1 + x/S$ (**Fig. 1**), which matches j at the discrete emitters and at the limits $x = \{0, L\}$:

$$\begin{cases} x = 0 & j^* = 1 \\ x = L & j^* = \frac{L}{S} + 1 = N + 1 \end{cases} \tag{12}$$

Thus, at any x, $j_* = 1 + x/S$, or at any j_*, $x = (j_* - 1)\,S$, the actual discharge flowing between the emitter j_* - 1 and j_* can be reasonably approximated to the average, Q_{j*}, between two contiguous emitters:

$$Q_{j_*} = q_n \frac{j_* - 1 + j_*}{2} = q_n \frac{1}{2}\left(1 + \frac{2x}{S}\right) \tag{13}$$

The average discharge, Q_{j*}, makes it possible to rewrite the energy balance equation applied over the interval [1, j_*] or [0, $(j_* - 1)/S$] as:

$$h_{j_*} = h_{min} + \frac{k\,S}{D^s} \int_1^{j_*} Q_{j_*}^r \, dj_* = h_{min} + \frac{k\,S\,q_n^r}{2^r\,D^s} \int_0^{(j_* - 1)\,S} \left(1 + \frac{2x}{S}\right)^r \frac{dx}{S} \tag{14}$$

where $dj_* = dx/S$. Applying the u-substitution, $(1 + 2\,x/S) = u$, the converted limits are:

$$\begin{cases} x = 0 & u = 1 \\ x & u = 1 + 2\frac{x}{S} = 1 + 2\,(j_* - 1) = 2\,j_* - 1 \end{cases} \tag{15}$$

Following the power rule and considering $dx = S/2\ du$, the integral over the interval [1, 2 j_* – 1] is:

$$h_u = h_{min} + \frac{k\, S\, q_n^r}{2^r\, D^s} \int_1^u \frac{u^r}{2}\, du = h_{min} + \frac{k\, S\, q_n^r}{2^{1+r}\, D^s} \frac{u^{r+1}}{r+1}\Bigg|_1^{2j_*-1} \tag{16}$$

yielding:

$$h_j = h_{min} + \frac{k\, S\, q_n^r (2j_* - 1)^{1+r} - 1}{D^s \quad 2^{1+r}\,(1+r)} = h_{min} + \frac{K\, S\, [(2\,j - 1)^{1+r} - 1]}{2^{1+r}\,(1+\, r)} \tag{17}$$

where on the right-hand side, j_* was replaced by j, and K (Eq. 6) can be expressed by using Eq. (7) or by Eq. (8).

By considering N-PCE emitters, N = 158 and S = 0.75 m (L = 118.5 m), for a uniform emitter flow rate q_n = 3.1 L/h associated with h_n = 20 m (**Fig. 2**), **Fig. 3** plots the comparison between the PHD obtained by Eq. (5) and by Eq. (17), clearly showing that Eq. (17) provides a PHD matching the exact one (Eq. 5).

Figure 3: ABOUT HERE.

It is important to note that, as in Eq. (5), for j = 1, Eq. (17) gives $h_1 = h_{min}$, whereas for $j = N + 1$, Eq. (17) provides the pressure heads that need to be applied at the inlet, h_{in} (**Fig. 1**):

$$h_{in} = h_{min} + K\, S \frac{(2\,N + 1)^{1+r} - 1}{2^{1+r}\,(1+\, r)} \tag{18}$$

To compare Eq. (10) and Eq. (18), which in practice are of greater interest than Eq. (5) (**Fig. 3**), we refer to the characteristics of cylindrical integrated in-line labyrinth emitters (TANDEM®) with double holes and turbulent flow provided by IRRITEC S.p.A., reported in **Table 1**, which are available commercially. It should be noted that these minor losses can only be neglected if the morphologies of the emitters do not produce significant reductions in the lateral cross-section, as do those of the start connectors (Martí et al., 2023).

Table 1: ABOUT HERE.

An error analysis was carried out to verify the suitability of Eq. (18). The inlet pressure head, h_{in} (Eq. 18), was calculated for 1,000 drip laterals characterized by different geometries and hydraulic parameters and compared with the exact value obtained via Eq. (10). A total of 1000 simulations were performed by randomly varying the emitter characteristics D, S, k_e, and x (reported in **Table 1**), N and h_{min} in the range [15, 500] and [5 m, 40 m], respectively, and by varying K (Eq. 6) with q_n (expressed by Eq. (1a)) and $h_n = h_{min}/(1\text{-}\delta)$ (Eq. 3). The pressure head tolerance, δ, was also randomly sampled around the commonly accepted 10% value (δ = 0.07, 0.08, 0.09, 0.1, 0.11, 0.12, 0.13). **Fig. 4a** shows the relative error RE(h_{in}) in computing the approximated h_{in}, $h_{in}^{(apx)}$, by Eq. (18) compared with the exact one, $h_{in}^{(ex)}$ (Eq. 10):

$$\mathrm{RE}(h_{in}) = \frac{h_{in}^{(apx)} - h_{in}^{(ex)}}{h_{in}^{(ex)}} \qquad (19)$$

Figure 4: ABOUT HERE.

Fig. 4a clearly indicates that Eq. (18) is an excellent approximation of the exact inlet pressure head (Eq. 10), with a negligible standard error of the estimate (SEE = 0.0001812 m), and allows the determination of an explicit solution of the number of emitters, N (as well as of the lateral length $L = N\,S$), which cannot be derived by the exact equation (Eq. 10).

Eq. (18) could be further simplified by considering that the term -1 is negligible compared to $(2\,N+1)^{1+r}$, especially for high N, thus providing:

$$h_{in} = h_{min} + \frac{K\,S}{1+r}\left(\frac{2\,N+1}{2}\right)^{1+r} \tag{20}$$

For the same dataset considered in **Fig. 4a**, the relative error associated with Eq. (20) is illustrated in **Fig. 4b**, indicating that using Eq. (20) in place of Eq. (17) yields a negligible higher error in computing h_{in} (SEE = 0.0001852 m) but with the benefit of more easily lending itself to further development, such as extending the one-lateral unit design to rectangular units (Baiamonte, 2018b).

Note that in Eqs. (10), (18) and (20), h_{min}, h_{in} and $K\,S$ are common factors in the three equations that can be made explicit with respect to $(h_{in} - h_{min})/(K\,S)$. Thus, to compare Eqs. (10, 18 and 20), the dependent variable $(h_{in} - h_{min})/(K\,S)$ can be plotted versus the number of emitters N, as shown in **Fig. 5a** for the Hazen–Williams resistance equation and in **Fig. 5b** for the Blasius resistance equation. The figures show that Eqs. (10, 18 and 20) provide similar results. Furthermore, substantial relative errors, RE (**Fig. 5c**), with respect to the exact solution (Eq. 10), only occur for low N values, which are not a concern in practice. For $N > 10$, the RE is less than 0.2%, which makes the proposed solutions suitable for use in practice. As shown in **Fig. 5c**, the Blasius equation provides a slightly smaller error than does the Hazen–Williams resistance equation.

Figure 5: ABOUT HERE.

By using Eq. (2) and Eq. (3), the nominal emitter pressure head, h_n, the inlet pressure head h_{in}, and the number of emitters, N, can be easily derived by Eq. (20) as a function of the pressure head tolerance, δ, which can be imposed in the drip lateral design:

$$h_n = \frac{K\,S\,[(2\,N+1)^{1+r}]}{2^{2+r}\,(1+r)\,\delta} \tag{21}$$

$$h_{in} = \frac{1+\delta}{\delta} K\, S \frac{(2\,N+1)^{1+r}}{2^{2+r}\,(1+r)} \tag{22}$$

$$N = \frac{1}{2}\left[\left(\frac{2^{2+r}\,(1+r)\,\delta\, h_{in}}{(1+\delta)\,K\,S}\right)^{\frac{1}{1+r}} - 1\right] \tag{23}$$

The relationship of the average pressure head, h_n, was also given in Baiamonte (2018a; see Eq. 24a), although it was obtained via calibration. A calibration coefficient F_0 that depends on the resistance equation (F_0 = 1.85, 1.83, and 1.81 for Blasius, Hazen-Williams and Darcy Weisbach, respectively) was considered. It is interesting to observe that the latter and the closed-form solution expressed by Eq. (21) provided very similar results, as can be easily verified, $(2\,N+1)^{1+r}/[2^{2+r}\,(1+r)] \cong (N/F_0)^{1+r}$.

Neglecting local losses (non-uniform emitter flow rate)

By neglecting local losses, the solution derived in the previous section (Eq. 23) makes it possible to obtain relationships useful for detecting the desired length of the drip lateral when a commercial emitter (with $x > 0$, i.e., a nonuniform emitter flow rate) is considered. The K parameter, involving the emitter flow rate (Eq. 6), needs to be substituted into Eq. (23), which allows the lateral length to be expressed as:

$$L = N\,S = \frac{S}{2}\left[\left(\frac{2^{2+r}\,(1+r)}{k\,S}\Psi\right)^{\frac{1}{1+r}} - 1\right] \tag{24}$$

where the Ψ function is equal to:

$$\Psi = \frac{\delta\, D^s\, h_{in}}{(1+\delta)\, q_n^r} \tag{25}$$

For the selected emitters' interspace, S (**Table 1**), and the Hazen-Williams resistance equation (r = 1.852, Eq. 8), Eq. (24) is plotted in both **Fig. 6a** and **Fig. 6b** as a function of Ψ. The Ψ function expressed in Eq. (25) can only be applied to PCE emitters, for which the emitter flow rate, q_n, does not depend on the emitter pressure head.

Figure 6: ABOUT HERE.

To detect the characteristics of commercial N-PCE emitters and evaluate the corresponding values of the Ψ function, the average pressure head, h_n, is needed, and two different design cases can be distinguished: case A), the inlet pressure head, h_{in}, is fixed and the emitter flow rate, q_n, is unassigned; and case B), the emitter flow rate, q_n, is fixed and the inlet pressure head is unassigned. Of course, for both cases, the emitter flow relation of the commercial emitter needs to be considered.

For case A) (h_{in} imposed), we substitute Eq. (1), with h_n expressed by Eq. (3) ($h_n = h_{in}/(1+\delta)$), into Eq. (25), yielding:

$$\Psi = \Psi_{h_{in}} = \frac{\delta\, D^s}{k_e^r}\left(\frac{h_{in}}{1+\delta}\right)^{1-rx} \qquad (26)$$

For case B) (q_{in} imposed), we substitute h_{in} expressed by Eq. (2) ($h_{in} = h_n\,(1+\delta)$), with h_n expressed by Eq. (1), into Eq. (25), yielding:

$$\Psi = \Psi_{q_n} = \frac{\delta\, D^s}{k_e^r}\left(\frac{q_n}{k_e}\right)^{\frac{1}{x}-r} \qquad (27)$$

where $\Psi_{h_{in}}$ and Ψ_{q_n} denote the Ψ function for the h_{in}-imposed or q_n-imposed case, respectively.

347 **Fig. 6a** and **Fig. 6b** also plot the vertical lines corresponding to the Ψ values (Eq. 26 and Eq. 348 27) for h_{in} = 22 m and q_n = 3.1 L/h, respectively, and for the Hazen-Williams resistance equation 349 associated with the commercial emitters reported in **Table 2**. The codes 13/1, 13/2, etc.,, were 350 assigned to each emitter. For any drip lateral length, **Fig. 6a** and **Fig. 6b** allow easy detection of 351 commercial emitters that ensure that, for a fixed inlet pressure (**Fig. 6a**) or for a fixed emitter flow 352 rate (**Fig. 6b**), the PHD matches the assumed pressure head tolerance (δ = 10%, **Table 3**). In **Fig. 6**, 353 the red dot indicates that for the 13.8/2 emitter (k_e = 0.69 L h^{-1} m^{-x} and x = 0.5), the lateral length 354 matches that considered in **Fig. 3** (L = 118.5 m), verifying Eq. (26) and Eq. (27).

355 An error analysis was also carried out to detect the influence of assuming a uniform emitter 356 flow rate for N-PCE emitters. For the same dataset considered in **Fig. 4** and for the lateral length 357 calculated by using the procedure described in the previous section, the relative error, RE, in the inlet 358 pressure head, h_{in}, compared to that derived by the exact step-by-step (SBS) procedure was calculated.

359 **Fig. 7** graphs the relative error RE (Eq. 19) versus the simulation number for the Hazen-360 Williams (**Fig. 7a**) and for the Blasius resistance equation (**Fig. 7b**), indicating that if the emitter flow 361 rate is not uniform but varies along the drip lateral according to the emitter flow relation (Eq. 1a), the 362 RE is less than 2.5%, thus suggesting that the proposed procedure is suitable for application in 363 practice, including for N-PCE emitters.

364

365 Figure 7: ABOUT HERE.

366

367 **Considering local losses (uniform emitter flow rate)**

368

369 Under a uniform emitter flow rate, when considering local losses due to emitter insertion, Eq. 370 (20) needs to be modified as:

371

$$h_{in} = h_{min} + \frac{K\,S}{1+r}\left(\frac{2\,N+1}{2}\right)^{1+r} + \alpha\,K_L\,H(N,-2) \tag{28}$$

where the last term accounts for the local losses expressed as a fraction of the kinetic head K_L:

$$K_L = k_L \frac{q_n^2}{D^4} \qquad \text{with } k_L = \frac{8}{g\,\pi^2} \tag{29}$$

and $H\,(N,-2)$ is the generalized harmonic of order $-\,2$, truncated at N:

$$H(N,-2) = \sum_{j=1}^{N} j^2 \tag{30}$$

Eq. (30) is a special case of Faulhaber's formula (Bazsó et al., 2012) and can be easily expressed as square pyramidal numbers:

$$H(N,-2) = \frac{1}{6} N\,(N+1)(2\,N+1) \tag{31}$$

Substituting Eq. (31) into Eq. (28) yields:

$$h_{in} = h_{min} + \frac{K\,S}{1+r}\left(\frac{2\,N+1}{2}\right)^{1+r} + \alpha\,K_L\,\frac{N}{6}\,(1+N)(1+2\,N) \tag{32}$$

For the case α = 0 (neglecting local losses), Eq. (32) cannot be made explicit with respect to N. However, for this PCE case ($x = 0$), after simple algebra and using Eq. (3), Eq. (32) can be rewritten to express the nominal pressure head, h_n, as a function of the pressure head tolerance δ:

$$h_n = \left(\frac{1+\,2\,N}{12\,\delta}\right)\left[\frac{3\,K\,S}{1+r}\left(\frac{1+\,2\,N}{2}\right)^r + \alpha\,K_L\,N\,(1+N)\right] \tag{33}$$

For a lateral with an emitter interspace S = 0.75 m and for different pairs (q_n, D), Eq. (33) is plotted versus the lateral length ($L = S\,N$) for α = 0.05 (**Fig. 8a**) and for α = 0.4 (**Fig. 8b**). **Fig. 8** allows easy determination of the required inlet pressure head by h_n ($h_{in} = (1 + \delta)\,h_n$) to be applied at the inlet. When minor losses are negligible (**Fig. 8a**), the inlet pressure head is quite close to that of **Fig. 3** ($h_{in} = h_n\,(1 + \delta) = 22$ m), whereas for α = 0.4 (**Fig. 8b**), because of relevant minor losses, a higher inlet pressure head ($h_{in} = h_n\,(1 + \delta) = 26.4$ m) is needed.

Figure 8: ABOUT HERE.

Considering local losses (non-uniform emitter flow rate)

For the previous case (N-PCE, $x > 0$), when local losses are considered, the K parameter (Eq. 6) and the K_L parameter (Eq. 30), involving the emitter flow rate Eq. (1), need to be considered in Eq. (33):

$$h_n = \left(\frac{1+\,2\,N}{12\,\delta}\right)\left[\frac{3\,k\,q_n^r\,S}{(1+r)\,D^s}\left(\frac{1+\,2\,N}{2}\right)^r + \alpha\,k_L\,\frac{q_n^2}{D^4}N\,(1+N)\right] \tag{34}$$

By using Eq. (1), to account for the emitters' characteristics k_e and x, because of the different exponents in the two terms, r and 2, Eq. (34) cannot be made explicit with respect to h_n (appearing in Eq. 1a), h_{in}, or k_e. By considering Eq. (1), Eq. (34) can be made explicit with respect to δ:

$$\delta = \left(\frac{1+2\,N}{12\,h_n}\right)\left[\frac{3\,k\,k_e^r\,h_n^{r\,x}\,S}{(1+r)\,D^s}\left(\frac{1+2\,N}{2}\right)^r + \alpha\,k_L\,\frac{k_e^2\,h_n^{2\,x}}{D^4}N\,(1+N)\right] \tag{35}$$

which makes it possible to graph δ versus lateral length, L, for a fixed h_n, α and emitter interspace S, as shown in **Fig. 9a**, for the considered commercial emitters in **Table 2**. Of course, for any pair (δ, h_n), h_{min} and h_{max} can be determined by Eq. (2). As might be expected, for any commercial emitter, as δ increases, longer drip laterals can be designed, but at the expensiveness of the emission uniformity.

Fig. 9: ABOUT HERE.

This is the case for the parameters previously considered (see code 13.8/2, D = 13.8 mm, S = 0.75 m, L =118.5 m, **Fig. 3**), where in **Fig. 9a**, it can be observed that the pressure head tolerance increases from 0.1 to 0.122 because of the local losses. **Fig. 9b** shows the linear dependency of the pressure head tolerance, δ, on the fraction of the kinetic head, α, where for the emitter with code 13.8/2, α = 0 and α = 0.05 correspond to δ = 0.1 and δ = 0.122, respectively.

To explore the influence of the uniform flow rate assumption, also in the case where minor losses are considered, 2,500 simulations were performed to calculate the relative error, RE(h_{in}), between the inlet pressure head under uniform and non-uniform (SBS) emitter flow rates. Simulations were performed by randomly varying δ, N, h_{min}, and α in the ranges [0.01 - 0.13], [15 - 500], [5 m - 40 m], and [0.1 - 0.8], respectively.

The results illustrated in **Fig. 10a** show that for some cases, the RE(h_{in}) is greater than the threshold of 2.5% observed when minor losses are neglected and may reach 14.8%, suggesting that this simplified procedure is not suitable.

Figure 10: ABOUT HERE.

However, it should be noted that most of the cases lay in between the line confining RE(h_{in}) = 2.5%, as can be observed in **Fig. 10b**, where the comparison between h_{in} approximated, $h_{in}^{(apx)}$, and exact, $h_{in}^{(ex)}$, is plotted, and in **Fig. 11**, where the corresponding RE(h_{in}) frequency distribution is displayed.

Fig. 11: ABOUT HERE.

The few cases in which high RE(h_{in}) values occur are likely due to low S values, and high L values are randomly sampled (high N values). To confirm this, simulations were performed by limiting N in the range $15 < N < 300$ (**Fig. 12a**). The results show that for this N range, RE(h_{in}) is less than 2.5%, as can also be observed in the one-by-one plot (**Fig. 12b**).

Figure 12: ABOUT HERE.

Finally, for one of the performed simulations with RE(h_{in}) = 0.019 < 2.5% (**Fig. 12**, red dots), by using Eq. (32) with $N = j - 1$, the PHD was determined by imposing $\delta = 0.122$ derived by Eq. (35) and indicated in **Fig. 9a** ($h_n = 20$ m, $S = 0.75$ m, $\alpha = 0.4$). The results are shown in **Fig. 13**, where the approximated PHD can be compared with that derived by the SBS method, demonstrating the consistency of Eq. (35), resulting in $h_{in}^{(ex)} = (1 + \mathrm{RE})\ h_{in}^{(apx)} = 1.019 \cdot 22.01 = 22.44$ m. The latter allows us to conclude that when local losses are considered, the suggested simple procedure can be applied for $N < 300$ to assure RE(h_{in}) < 2.5%, whereas there are no N limitations if local losses are neglected, provided $\delta < 0.13$ (i.e., the highest value considered in simulations).

Fig. 13: ABOUT HERE.

As a final remark, the maximum error of 2.5% is of overpressure (RE(h_{in}) > 0), which would favour plant wellbeing in the low range of pressure heads. Indeed, imposing a slightly overestimated

h_{in}, in the exact SBS procedure, results in a slight h_{min} overestimation and a slightly greater pressure head in the low range of pressure heads, thereby supplying a slightly greater water volume.

Conclusions

The most important points covered in this paper are summarized as follows:

- For laterals laid on relatively flat fields, a simple design relationship previously introduced under the assumption of uniform emitter flow rates and by using calibration factors was analytically derived in a closed-form, with results matching those derived by the exact step-by-step procedure. It is shown that if i) the pressure head tolerance is sufficiently small (< 0.13) and ii) the uniform flow rate to be selected for the emitters is associated with the nominal (average) pressure head, the error in computing the inlet pressure head is less than 2.5%. The suggested design procedure is very simple and can be applied for non-pressure compensating emitters to determine the inlet pressure head, if the emitter flow rate is assigned, or to the emitter flow rate, if the inlet pressure head is established.
- For an assigned pressure head tolerance, the characteristics of the commercial emitters required to achieve the designed drip lateral can easily be detected.
- In the case in which minor losses are considered, to obtain a relative error in the inlet pressure head of less than 2.5%, the number of emitters must not exceed 300.

ACKNOWLEDGEMENTS

The author wishes to thank the Editor Professor Jiusheng Li and the anonymous reviewers for their helpful comments and suggestions made during the revision stage.

DATA AVAILABILITY STATEMENT

The data are available from the author upon reasonable request.

REFERENCES

Abramowitz M., and Stegun I.A. 1965. *Handbook of Mathematical Functions with Formulas, Graphs, and Mathematical Tables*. Dover Publications Inc., New York, 1046 p.

Baiamonte G. 2016a. Simple Relationships for the Optimal Design of Paired Drip Laterals on Uniform Slopes. *Journal of Irrigation and Drainage Engineering-ASCE*, **142**(2), Doi: 10.1061/(ASCE)IR.1943-4774.0000971, 04015054.

Baiamonte G. 2016b. Closure to "Simple Relationships for the Optimal Design of Paired Drip Laterals on Uniform Slopes" by Giorgio Baiamonte, *Journal of Irrigation and Drainage Engineering-ASCE*, **142**(12), Doi: 10.1061/(ASCE)IR.1943-4774.0001126, 07016019.

Baiamonte G. 2018a. Advances in designing drip irrigation laterals. *Agricultural Water Management*, **199**:157–174. https://doi.org/10.1016/j.agwat.2017.12.015.

Baiamonte G. 2018b. Explicit Relationships for Optimal Designing of Rectangular Microirrigation Units on Uniform Slopes: the IRRILAB Software Application. *Computers and Electronics in Agriculture*, **153**:151-168. https://doi.org/10.1016/ j.compag.2018.08.005.

Baiamonte G., Palermo S., Sadeghi S.H., and Peters, R.T. 2024. Design Emission Uniformity of Horizontal Tapered Drip Laterals from the Normalized Pressure Head Distribution Approach. *Journal of Irrigation and Drainage Engineering-ASCE*. Doi: 10.1061/JIDEDH/IRENG-10300.

Bazsó A., Pintér Á., and Srivastava H.M. 2012. A refinement of Faulhaber's theorem concerning sums of powers of natural numbers. *Applied Mathematics Letters,* **25**: 486–489.

Dercas N., and Valiantzas J.D. 2012. Two explicit optimum design methods for a simple irrigation delivery system: comparative application. *Irrigation and Drainage,* **61**: 10–19.

Foley J.A., Ramankutty N., Brauman K.A., Cassidy E.S., Gerber J.S., Johnston M., Mueller N.D., O'Connell C., Ray D.K., West P.C., Balzer C., Bennett E.M., Carpenter S.R., Hill J., Monfreda C., Polasky S., Rockström J., Sheehan J., Siebert S., Tilman D., and Zaks D.P. 2011. Solutions for a cultivated planet. *Nature*, **478**(7369): 337–342. https://doi. org/ 10. 1038/ nature10452.

Friedlander L., Tal, A., and Lazarovitch N. 2013. Technical considerations affecting adoption of drip irrigation in sub-Saharan Africa. *Agricultural Water Management*, **126**:125-132. https://doi.org/10.1016/j.agwat.2013.04.014.

Kang Y., and Nishiyama S. 1996. Analysis and design of microirrigation laterals. *Journal of Irrigation and Drainage Engineering-ASCE*, **122**(2), 75-82.

Karmeli D., and Keller J. 1975. *Trickle Irrigation Design. Rain Bird Sprinkler Manufacturing Corporation*, Glendora, Calif.

Liu H., Duan A.W, Li F.S., Sun J.S., Wang Y.C., and Sun C.T. 2013. Drip irrigation scheduling for tomato grown in solar greenhouse based on pan evaporation in North China Plain, *Journal of Integrative Agriculture*, **12**(3):520-531. https://doi.org/10.1016/S2095-3119(13)60253-1.

Martí P., Shiri J., Román A., Turégano J.V., and Royuela A. 2023. Analysis of local head losses in microirrigation lateral connectors based on machine learning approaches. *Irrigation Science*, **41**:783-801. https://doi.org/10.1007/s00271-023-00852-z.

Moghazi H.E.D.M. 1998. Estimating Hazen-Williams Coefficient for Polyethylene Pipes. *Journal of Transportation Engineering*, **124**:197-199.

Rodell M., and Li. B. 2023. Changing intensity of hydroclimatic extreme events revealed by GRACE and GRACE-FO. *Nat Water* **1**, 241–248. https://doi.org/10.1038/s44221-023-00040-5.

Shareef T., Ma Z., and Zhao B. 2019. Essentials of Drip Irrigation System for Saving Water and Nutrients to Plant Roots: As a Guide for Growers. *Journal of Water Resource and Protection*, **11**:1129-1145. doi: 10.4236/jwarp.2019.119066.

Singh V.P., and Su Q. 2022. Irrigatio*n Engineering. Principles, Processes, Procedures, Design, and Management*. Cambridge, University Press, UK.

Valiantzas J.D. 1998. Analytical approach for direct drip lateral hydraulic calculation. *Journal of Irrigation and Drainage Engineering-ASCE*, **124**(6), 300-305.

Warrick A.W., and Yitayew M. 1988. Trickle lateral hydraulics. I: Analytical solutions. *Journal of Irrigation and Drainage Engineering-ASCE*, **114**(2): 281–288.

Wu I.P. 1992. Energy gradient line approach for direct hydraulic calculation in drip irrigation design. *Irrigation Science*, **13**:21-29.

Wu I.P., Howell T.A., and Hiler E.A. 1979. Hydraulic design of drip irrigation systems. Hawaii agricultural experiment station. Technical bulletin. Vol. 105, 80. Honolulu: University of Hawaii.

Yitayew M., and Warrick A.W. 1988. Trickle lateral hydraulics. II: Design and examples. *Journal of Irrigation and Drainage Engineering-ASCE*, **114**(2): 289-300.

List of figures

Fig. 1. Sketch of a drip lateral considered in this work. The nominal (average) pressure head, h_n, and the maximum and minimum pressure heads, h_{min} and h_{max}, depending on the pressure head tolerance, δ, are indicated.

Fig. 2. For $k_e = 0.69$ L h^{-1} m^{-x} and $x = 0.5$, an example of the pressure head – emitter flow rate (PH-FL) relationship. According to $h_n = 20$ m, for $\delta = 0.1$, the range of variability of the pressure head distribution (PHD), $[h_{min}, h_{max}]$, is reported.

Fig. 3. Comparison between the pressure head distribution (PHD) obtained by Eq. (17) and that derived by Eq. (5) for the parameters indicated in the figure, for pressure-compensating emitters (PCEs), and neglecting local losses.

Fig. 4. Relative error in the inlet pressure head, RE(h_{in}), calculated a) by Eq. (18) and b) by Eq. (20), with respect to that obtained by the exact Eq. (5) for the 1000 random simulations performed for PCEs and for different random combinations of D, S, k_e, x, N, q_n, h_{min} and δ.

Fig. 5. Comparison between $(h_{in} - h_{min})/(K\ S)$ derived from Eqs. (10, 18 and 20) vs. the number of emitters, N, a) for Hazen-Williams, and b) for the Blasius resistance equation for PCEs and neglecting local losses. For both resistance equations, c) the relative errors, RE, calculated with respect to the exact $(h_{in} - h_{min})/(K\ S)$ of Eq. (10), are also reported.

Fig. 6. Drip lateral length, L, vs. the Ψ parameter (Eq. 24), for different emitter interspaces, S, for PCEs and when neglecting local losses. For the considered commercial emitters (Table 3), the vertical lines indicate a) the $\Psi_{h_{in}}$ parameter and b) the Ψ_{q_n} parameter to be used if q_n or h_n is fixed, respectively.

Fig. 7. For 1,000 random simulations performed for different D, S, k_e, x, N, q_n, h_{min}, and δ, for N-PCEs and by neglecting local losses, a) the relative error in the inlet pressure head, RE(h_{in}), with

respect to that obtained by the exact SBS procedure, a) under Hazen-Williams and b) under Blasius resistance equations.

Fig. 8. Nominal (average) emitter pressure head, h_n, for PCEs and considering local losses, calculated by Eq. (33) vs. the lateral length, L, for the inside diameter of the considered commercial emitters (Table 3), and for different q_n values, a) for α = 0.05, and b) for α = 0.4. The red dot refers to the application of Fig. 3.

Fig. 9. Relationship between the pressure head tolerance, δ, a) for fixed α, vs. the lateral length, L, and b) for fixed $L = N\,S = 118.5$ m, vs. the α parameter, for N-PCEs and considering local losses, for the considered commercial emitters (Table 3). The red dot refers to the application of Fig. 3.

Fig. 10. For 2,500 random simulations ($15 < N < 500$), for N-PCEs, and considering local losses, a) the relative error in the inlet pressure head, RE(h_{in}), with respect to that obtained by the exact SBS procedure, and b) comparison between the exact (SBS) and the approximated h_{in} (Eq. 36), with the line RE(h_{in}) = 2.5% also reported.

Fig. 11. Frequency distribution of RE(h_{in}), corresponding to Fig. 10, for $15 < N < 500$ and $N > 300$ emitters.

Fig. 12. For 2,500 random simulations ($15 < N < 300$), for N-PCEs, and considering local losses, a) relative error in the inlet pressure head, RE(h_{in}), with respect to that obtained by the exact SBS procedure and b) comparison between the exact (SBS) and the approximated h_{in} (Eq. 36), with the line of RE(h_{in}) = 2.5% also reported.

Fig. 13. Comparison between the PHD distribution derived by using Eq. (32), with δ = 0.122 (Eq. 35), and that derived by the exact SBS procedure for the parameters indicated in the figure for N-PCEs and considering local losses (α = 0.4).

Table 1 – Emitters' characteristics considered in this work

s (m)	ϕ (mm)	D (mm)	k_e (L h^{-1} m^{-x})	x	*emitter colour*
0.2	16	13.8	0.43	0.55	yellow
0.3			0.69	0.50	light blue
0.4			1.32	0.49	black
0.5			2.48	0.51	red
0.6	20	17.7	0.56	0.52	yellow
0.75			0.80	0.49	light blue
1.00			1.2	0.48	black
1.25			2.35	0.49	red
1.50			4.94	0.47	green

Table 2 – Minimum and maximum values of the parameters influencing the Ψ, $\Psi_{h_{in}}$, and Ψ_{q_n} functions and their corresponding values.

parameter	*Min*	*Max*
δ	0.07	1.3
D (mm)	13.8	17.7
k_e (L h^{-1} m^{-x})	0.43	4.94
x	0.47	0.55
q_n (L/h)	2	12
h_{in} (m)	5	40
Ψ	3.96	25,405
Ψ_{hin}	4.14	33,726
Ψ_{qn}	3.42	22,491

Table 3 – For $\delta = 0.1$, $h_{in} = 22$ m, $q_n = 3.1$ L/h, and for the considered emitters' characteristics, values of the Ψ parameters under the Blasius and Hazen-Williams resistance equations.

code	k_e (L h^{-1} m^{-x})	x	$r = 1.852$, $s = 4.871$, $\delta = 0.1$		$r = 1.75$, $s = 4.75$, $\delta = 0.1$	
			Ψ_{hin} ($h_{in} = 22$ m)	Ψ_{qn} ($q_n = 3.1$ L/h)	Ψ_{hin} ($h_{in} = 22$ m)	Ψ_{qn} ($q_n = 3.1$ L/h)
13.8/1	0.43	0.55	544.8	538.9	212.9	217.6
13.8/2	0.69	0.50	299.5	299.5	120.9	120.9
13.8/3	1.32	0.49	95.2	84.7	41.0	34.2
13.8/4	2.48	0.51	26.5	23.0	12.2	9.3
17.7/1	0.56	0.52	1,326	1,340	511.9	525.2
17.7/2	0.80	0.49	809.1	791.3	320.9	310.1
17.7/3	1.2	0.48	403.6	360.1	166.3	141.1
17.7/4	2.35	0.49	110.0	87.8	48.7	34.4
17.7/5	4.94	0.47	31.0	18.5	14.7	7.2

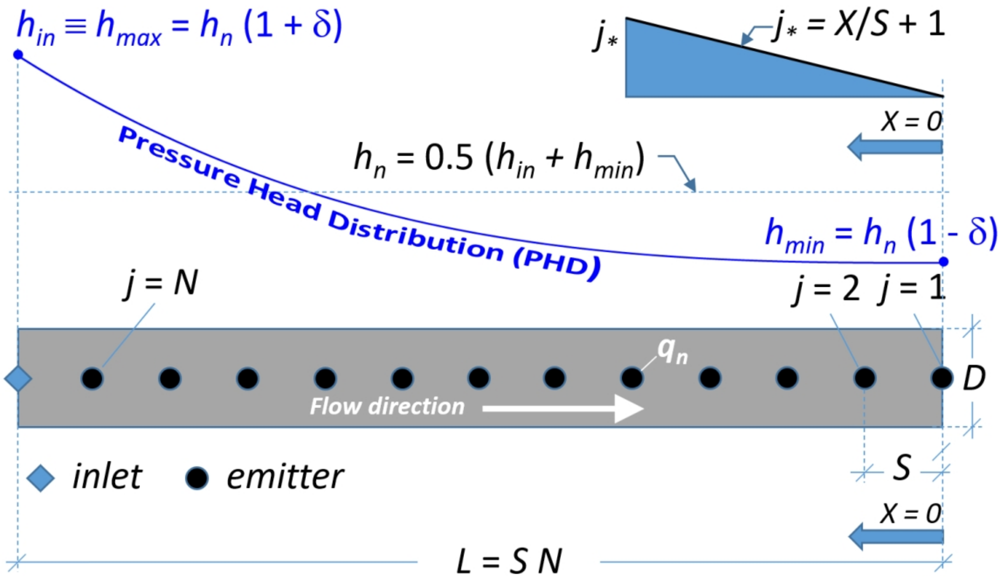

Fig. 1 – Sketch of a drip lateral considered in this work. The nominal (average) pressure head, h_n, and the maximum and minimum pressure heads, h_{min} and h_{max}, depending on the pressure head tolerance, δ, are indicated.

64x36mm (600 x 600 DPI)

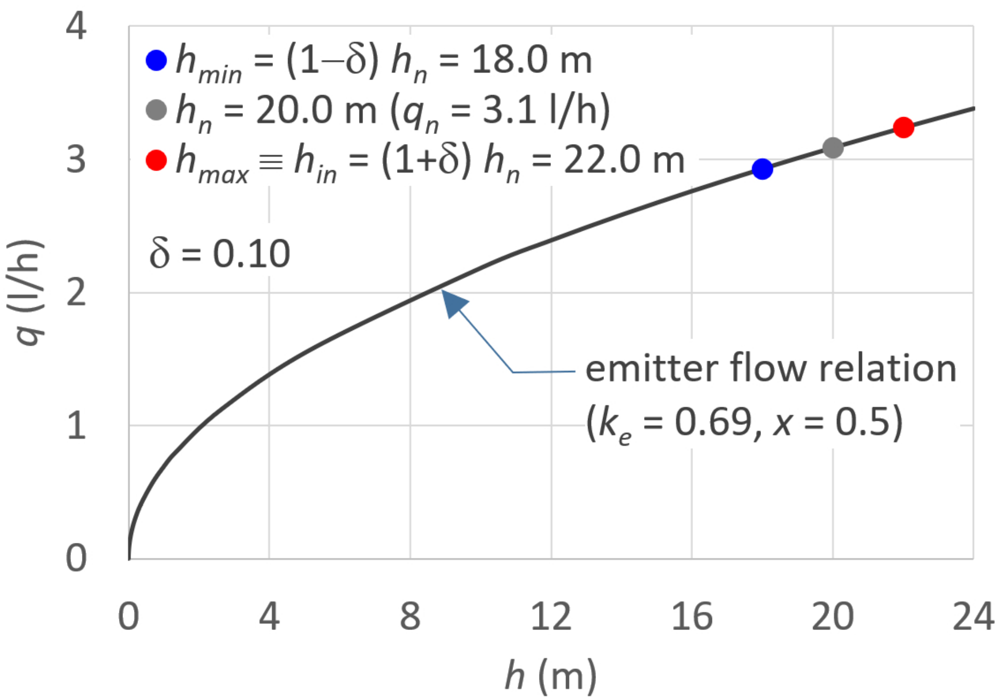

Fig. 2 – For k_e = 0.69 l h^{-1} m^{-x} and x = 0.5, example of the pressure head – emitter flow rate (PH-FL) relationship. According to h_n = 20 m, for δ = 0.1, the range of variability of the pressure head distribution (PHD), [h_{min}, h_{max}], is reported.

47x33mm (600 x 600 DPI)

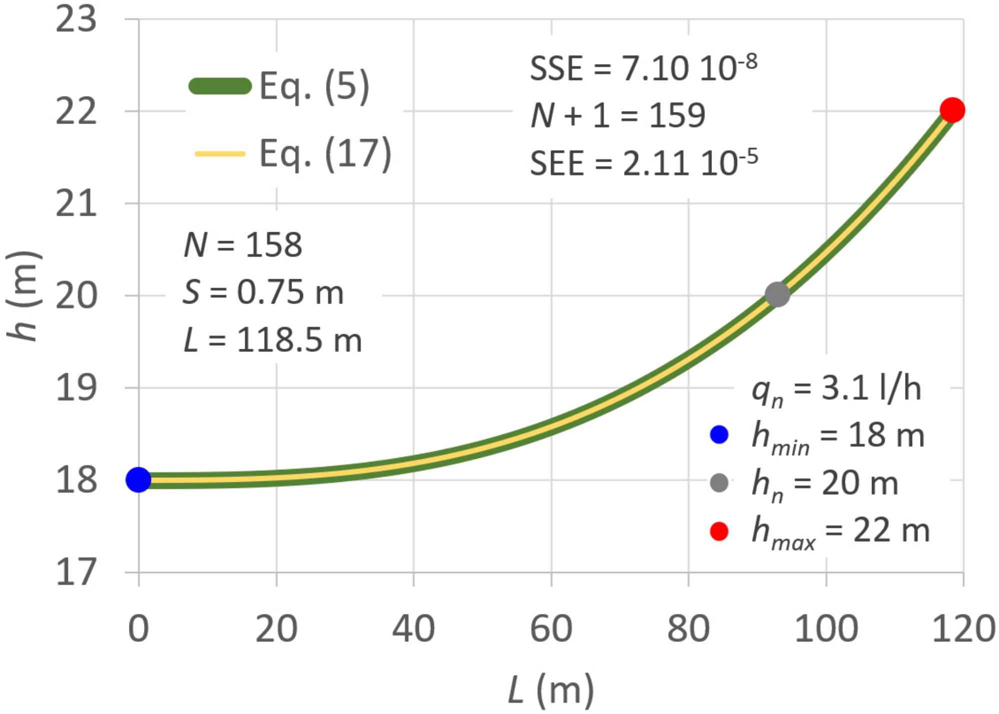

Fig. 3 – Comparison between the PHD obtained by Eq. (17) and that derived by the exact Eq. (5) for the parameters indicated in the figure, for pressure-compensating emitters (PCEs), and neglecting local losses.

47x34mm (600 x 600 DPI)

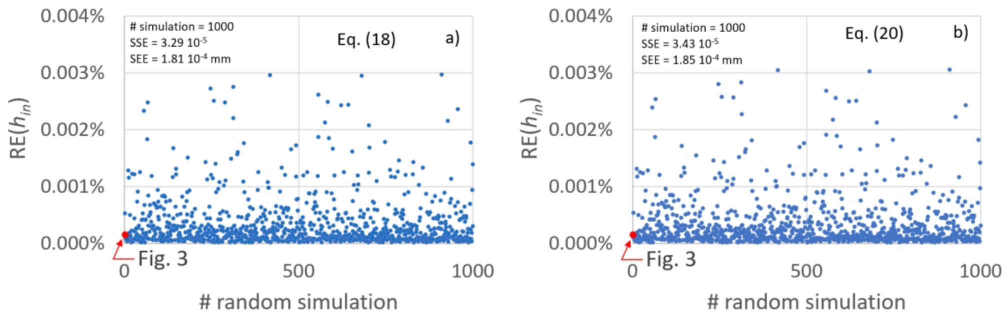

Fig. 4 – Relative error in the inlet pressure head, RE(h_{in}), calculated a) by Eq. (18) and b) by Eq. (20), with respect to that obtained by the exact Eq. (5) for #1000 random simulations performed for PCEs, and for different random combinations of D, S, k_e, x, N, q_n, h_{min} and δ.

76x23mm (600 x 600 DPI)

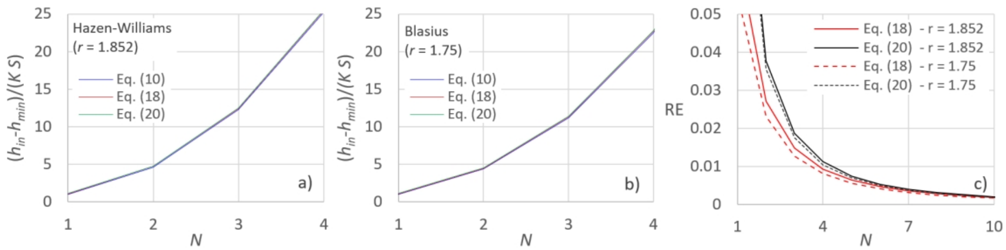

Fig. 5 – Comparison between (h_{in}-h_{min})/KS derived from Eqs. (10, 18 and 20) vs. the number of emitters, N, a) for the Hazen-Williams, and b) for the Blasius resistance equation, for PCEs and neglecting local losses. For both resistance equations, c) the relative errors RE, calculated with respect to the exact (h_{in}-h_{min})/KS of Eq. (10) is also reported.

77x18mm (600 x 600 DPI)

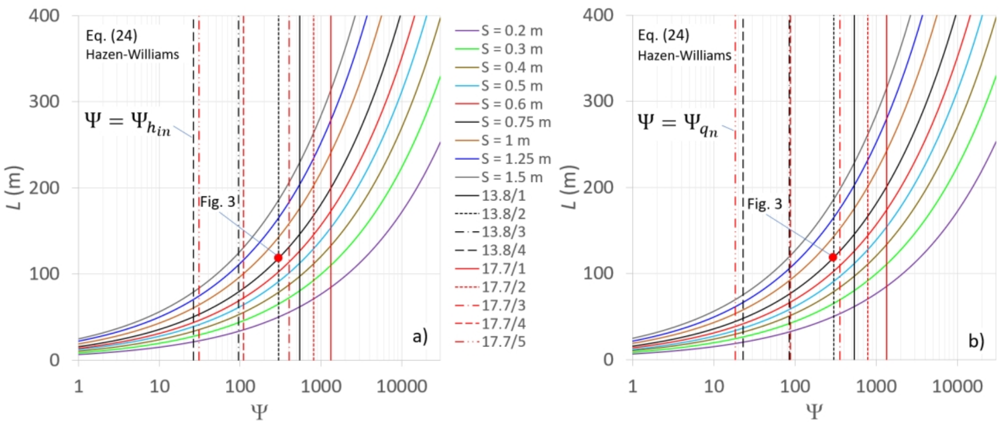

Fig. 6 - Drip lateral length, L, vs. the Ψ parameter (Eq. 24), for different emitter interspaces, S, for PCEs and when neglecting local losses. For the considered commercial emitters (Table 3), the vertical lines indicate a) the Ψ_{in} parameter and b) the Ψ_{qn} parameter, to be used if q_n or h_n is fixed, respectively.

75x31mm (600 x 600 DPI)

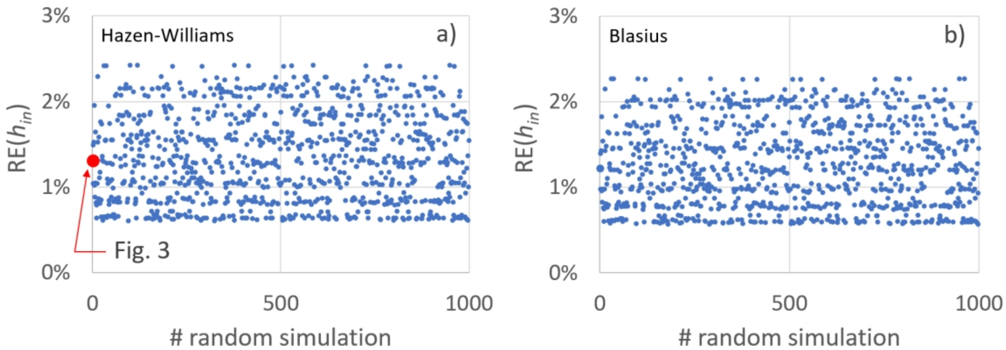

Fig. 7 – For #1,000 random simulations performed for different D, S, k_e, x, N, q_n, h_{min}, for N-PCEs, and by neglecting local losses, a) relative error in inlet pressure head, RE(h_{in}), with respect to that obtained by the exact SBS procedure, a) under Hazen-Williams and b) under Blasius resistance equations.

74x25mm (600 x 600 DPI)

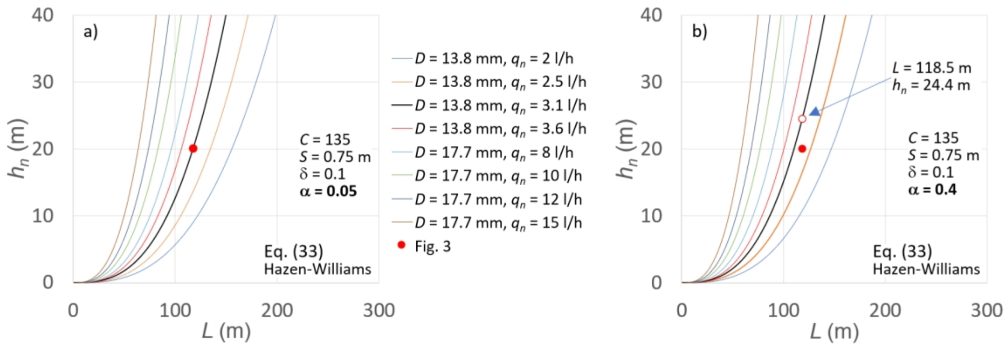

Fig. 8 – Nominal (average) emitter pressure head, h_n, for PCEs and considering local losses, calculated by Eq. (33) vs. the lateral length, L, for the inside diameter of the considered commercial emitters (Table 3), and for different q_n values, a) for α = 0.05, and b) for α = 0.4. The red dot refers to the application of Fig. 3.

76x25mm (600 x 600 DPI)

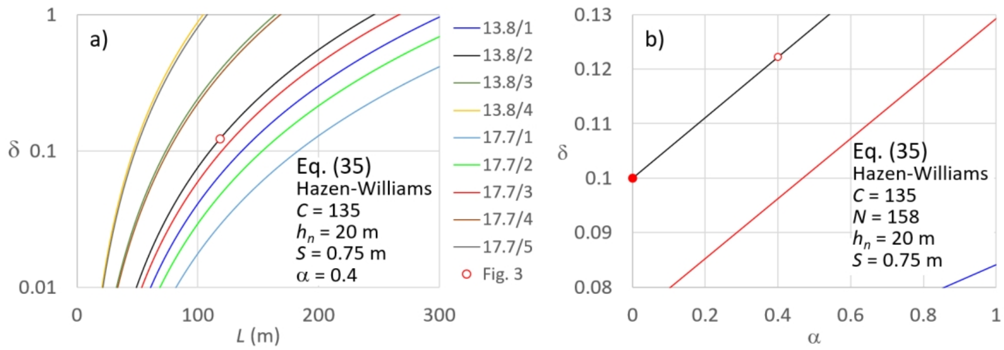

Fig. 9 – Relationship between the pressure head tolerance, δ, a) for fixed α, vs. the lateral length, *L*, and b) for fixed $L = N\,S = 118.5$ m, vs. the α parameter, for N-PCEs and considering local losses, for the considered commercial emitters (Table 3). The red dot refers to the application of Fig. 3.

73x25mm (600 x 600 DPI)

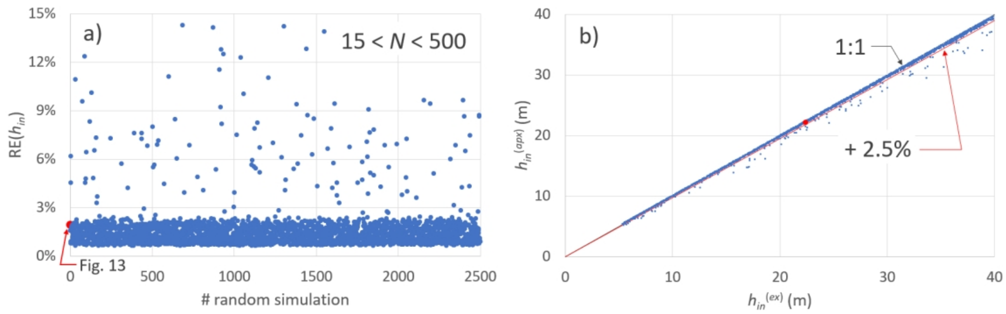

Fig. 10 – For 2,500 random simulations (15 < *N* < 500), for N-PCEs, and considering local losses, a) relative error in the inlet pressure head, RE(h_{in}), with respect to that obtained by the exact SBS procedure, and b) comparison between the exact (SBS) and the approximated h_{in} (Eq. 36), with the line RE(h_{in}) = 2.5 % also reported.

73x22mm (600 x 600 DPI)

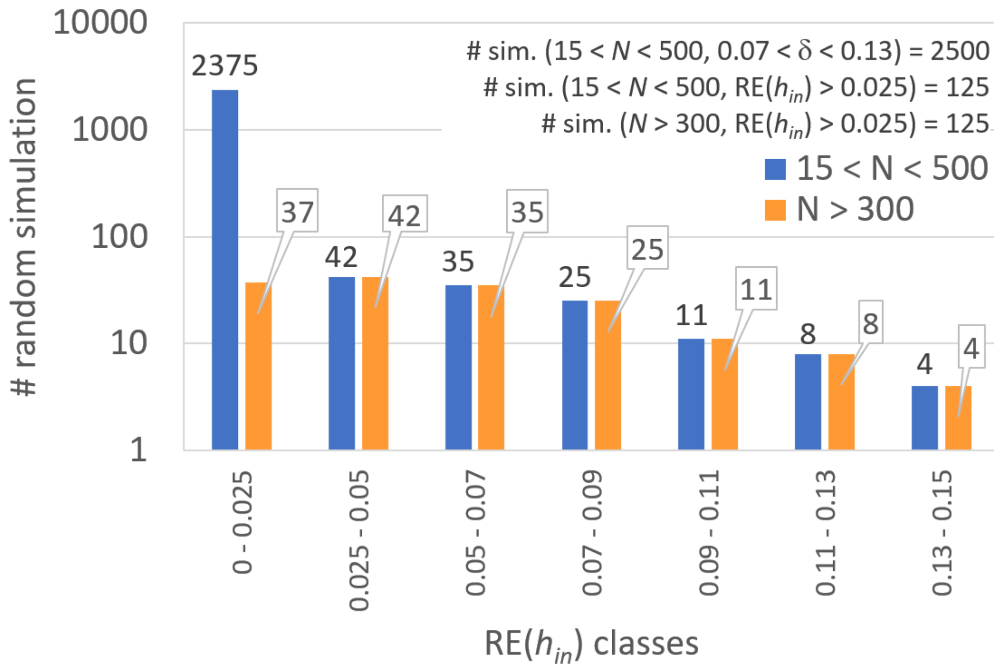

Fig. 11 – Frequency distribution of RE(h_{in}), corresponding to Figure 10, for 15 < N < 500 and N > 300 emitters.

46x30mm (600 x 600 DPI)

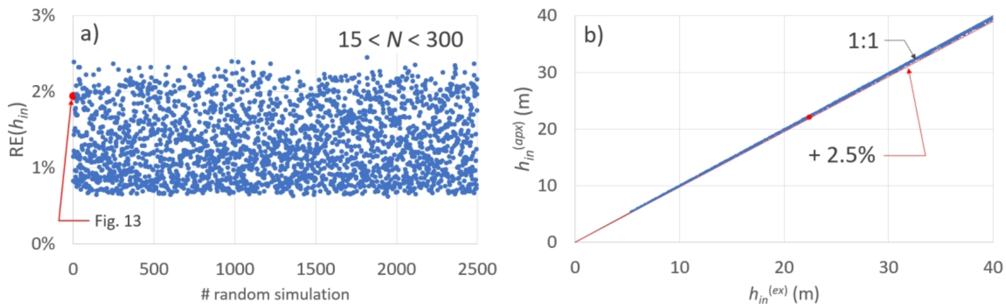

Fig. 12 – For 2,500 random simulations ($15 < N < 300$), for N-PCEs, and considering local losses, a) relative error in inlet pressure head, RE(h_{in}), with respect to that obtained by the exact SBS procedure, and b) comparison between the exact (SBS) and the approximated hin (Eq. 36), with the line of RE(h_{in}) = 2.5 % also reported.

73x22mm (600 x 600 DPI)

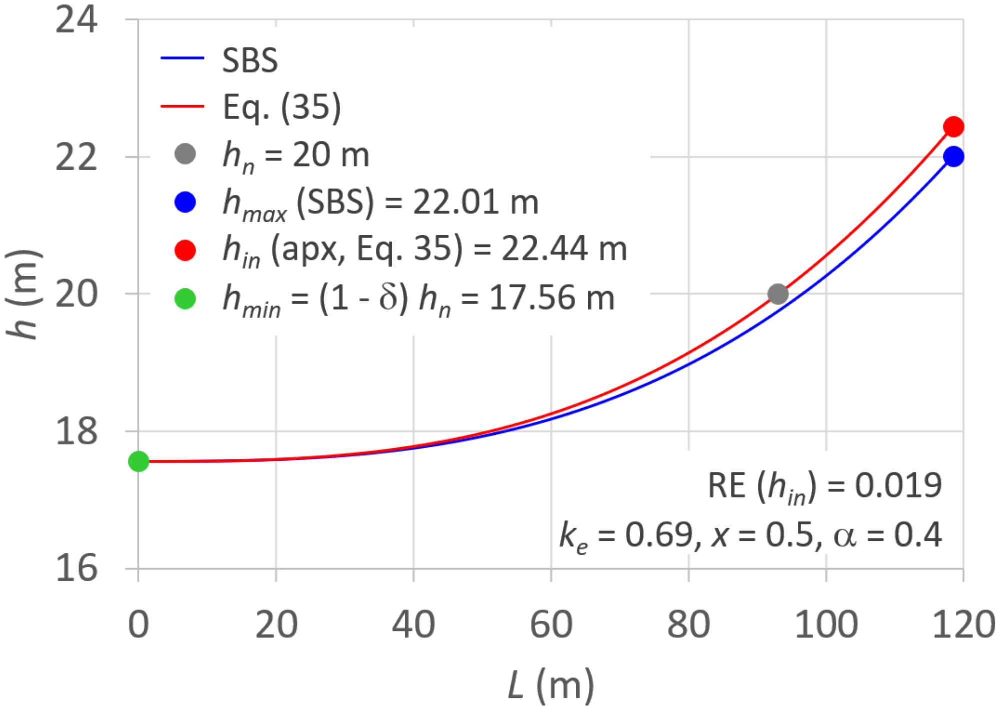

Fig. 13 – Comparison between the PHD distribution derived by using Eq. (32), with δ = 0.122 (Eq. 35) with that derived by the exact SBS procedure, for the parameters indicated in the figure, for N-PCEs and considering local losses (α = 0.4).

45x32mm (600 x 600 DPI)